Anomalously Hot Electrons due to Rescatter of Stimulated Raman Scattering in the Kinetic Regime

B. J. Winjum,[1] J. E. Fahlen,[2] F. S. Tsung,[3] and W. B. Mori[1,3]

[1]*Department of Electrical Engineering, University of California Los Angeles, Los Angeles, California 90095, USA*
[2]*Areté Associates, Northridge, California 91324, USA*
[3]*Department of Physics and Astronomy, University of California Los Angeles, Los Angeles, California 90095, USA*

(Received 18 September 2012; published 15 April 2013)

Using particle-in-cell simulations, we examine hot electron generation from electron plasma waves excited by stimulated Raman scattering and rescattering in the kinetic regime where the wave number times the Debye length ($k\lambda_D$) is $\gtrsim 0.3$ for backscatter. We find that for laser and plasma conditions of possible relevance to experiments at the National Ignition Facility, anomalously energetic electrons can be produced through the interaction of a discrete spectrum of plasma waves generated from stimulated Raman scattering (back and forward scatter), rescatter, and the Langmuir decay of the rescatter-generated plasma waves. Electrons are bootstrapped in energy as they propagate into plasma waves with progressively higher phase velocities.

DOI: 10.1103/PhysRevLett.110.165001 PACS numbers: 52.38.Bv, 52.35.Fp, 52.35.Mw, 52.65.−y

Stimulated Raman scattering (SRS), the decay of a light wave into a forward propagating electron plasma wave (EPW) and a forward (SRFS) or backward (SRBS) propagating light wave, involves fundamental nonlinear wave-wave and wave-particle interactions. SRS continues to be studied extensively because the loss of incoming energy due to backscatter and the potential fuel preheat due to hot electrons generated by the EPW are threats to inertial fusion energy devices such as the National Ignition Facility (NIF). Recent NIF experiments have shown electron heating up to energies above 100 keV [1]. A low-temperature ($T_e = 10$–20 keV) part of the heated electron distribution can be attributed to SRBS, but the high-temperature part is currently unexplained. There is speculation that these electrons are generated near the quarter-critical density by instabilities such as two-plasmon decay or SRFS [2].

In this Letter, we present a novel mechanism for generating 100 keV electrons through SRS rescatter, specifically through SRBS of SRBS, SRBS of SRFS, and the Langmuir decay instability (LDI) of rescatter EPWs, where LDI is the decay of an EPW into a counterpropagating EPW and an ion acoustic wave. We further show that electrons can get progressively heated as they travel between waves of increasing phase velocities. This mechanism allows rescatter and SRFS to heat electrons initially heated by SRBS, even though the SRFS EPW phase velocity is too high to trap and heat electrons on its own.

Particle-in-cell (PIC) simulations have been used to study rescatter and multistage electron heating from SRS, albeit with multistage heating between SRBS and SRFS. Hinkel *et al.* [3] showed rescattering for NIF-relevant parameters but not the resulting hot electrons. Other authors [4–7] have shown electron heating by SRFS, in some cases explicitly due to SRFS accelerating electrons initially heated by SRBS, but these simulations were for more intensely driven and/or hotter plasmas outside the current range for NIF where electron temperatures $T_e \approx 2$–6 keV and laser intensities I and wavelengths λ_0 are such that $I\lambda_0^2 \approx 10^{14}$ W μm^2/cm^2 (in laser hot spots).

Electron energies that result from trapped particle interactions depend on the EPW's phase velocity v_ϕ and potential amplitude Φ with the trapped electron with the highest energy being that which oscillates between the top and bottom of the wave's potential well with potential difference $\Delta\Phi$. The maximum velocity $v_{\max}$ and energy $\mathcal{E}_{\max}$ of a trapped electron can be obtained by considering that an electron's energy $\mathcal{E}$ is conserved in the wave ($'$) frame, with $\mathcal{E}' = (\gamma_v' - 1)mc^2 - e\Phi'$ where $\Phi' = \gamma_{v_\phi}\Phi$, $\gamma_v \equiv [1 - (v/c)^2]^{-1/2}$, and e and m are the electron charge and mass, respectively. In the nonrelativistic limit, $v_{\max}$ is found to be $v_\phi + \sqrt{2e(\Delta\Phi)/m}$ and $\mathcal{E}_{\max} = \frac{1}{2}mv_{\max}^2$. For a sinusoidal EPW, $\Delta\Phi = 2\Phi_{\max}$ and $v_{\max} = v_\phi + v_{\rm tr}$, with the trapping width $v_{\rm tr} = 2\sqrt{e\Phi_{\max}/m}$. Figure 1 illustrates trapped electrons oscillating between $v_{\max} = v_\phi \pm v_{\rm tr}$ in a kinetic SRS simulation (the first simulation below).

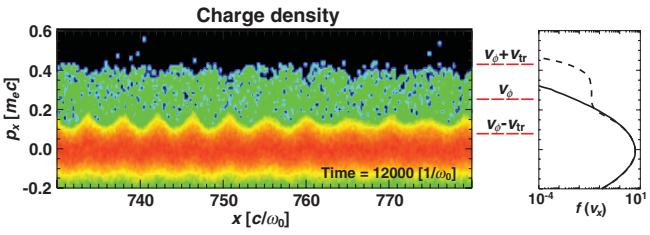

FIG. 1 (color). Electron phase space showing trapped particles during SRBS (left panel) with the corresponding flattening of the distribution function (right panel, dashed line) and initial distribution (right panel, solid line).

To estimate $\mathcal{E}_{\max}$ as a function of $k\lambda_D$, the EPW wave number times the Debye length, we assume the EPW amplitude is bounded by the warm wave breaking limit [8]. Since $v_{\max}$ and $\mathcal{E}_{\max}$ above depend on $\Delta\Phi$, we consider the wave breaking derivation of Ref. [9], which shows that extrema in $\Phi(\bar{v})$,

$$\Phi(\bar{v}) = -\bar{v} + \frac{\bar{v}^2}{2} + \frac{\bar{\beta}}{2(1-\bar{v})^2} + c_0, \tag{1}$$

occur for roots of $\bar{E}(\bar{v})$, where

$$(\bar{E}(\bar{v}))^2 = \bar{E}_{\text{peak}}^2 - \bar{v}^2 + \bar{\beta}\left[\frac{2}{3(1-\bar{v})^3} - \frac{1}{(1-\bar{v})^2} + \frac{1}{3}\right].$$

Here, a water-bag distribution is assumed, $\bar{E} = eE/m\omega_p v_\phi$ is the normalized electric field, $\bar{v} = v/v_\phi$, $\bar{\beta} = 3(v_{\text{th}}/v_\phi)^2 = 3k^2\lambda_D^2/(1+3k^2\lambda_D^2)$, and c_0 is an arbitrary constant. Assuming $\bar{E}_{\text{peak}}$ is the wave breaking amplitude, two of the roots correspond to fluid velocities at the extrema in Φ at wave breaking. We can substitute these two roots into Eq. (1) to calculate $\Delta\Phi$ between the extrema and substitute $\Delta\Phi$ into the above expressions for $v_{\max}$ and $\mathcal{E}_{\max}$ [10]. Figure 2 (top left panel) shows $v_{\max}/v_\phi$ as a function of β, from which it is seen that for $\beta > 0.1$ ($k\lambda_D \gtrsim 0.18$) the difference between $v_{\max}$ and v_ϕ is no bigger than v_ϕ, i.e., $v_{\max} < 2v_\phi$. Figure 2 (top right panel) shows $\mathcal{E}_{\max}$, assuming that $T_e = 2.5$ keV, where the dotted line uses $\mathcal{E}_{\max} = \frac{1}{2}mv_{\max}^2$ and the solid line includes relativistic corrections. In simulations, we find that E_{peak} (Φ_{peak}) for the SRBS wave is typically $\lesssim 2/3$ of the wave breaking estimate, so these curves should be viewed as a limit.

The appropriate v_ϕ and $\mathcal{E}_\phi$ values (kinetic energy for a particle at v_ϕ) for the various EPWs are shown in Fig. 2 (bottom panel). The plots in combination show that SRBS does not longitudinally accelerate electrons to 100 keV kinetic energies. Trapped particles with additional

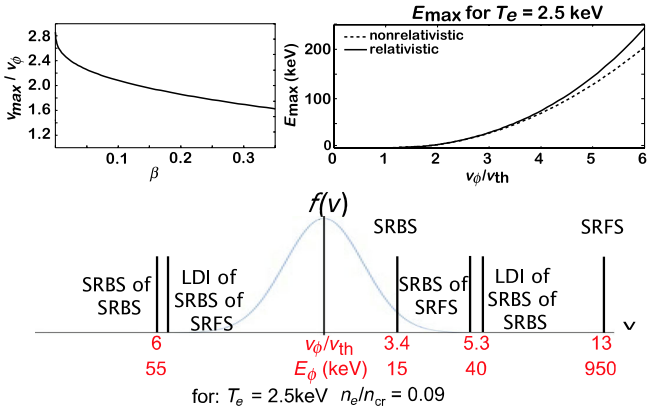

FIG. 2 (color online). Estimate of bound on maximum electron velocity $v_{\max}$ (top left) and kinetic energy $E_{\max}$ (assuming T_e = 2.5 keV, top right). EPW phase velocities for one set of parameters (bottom) illustrate the phase-velocity ordering of modes, with rescatter and LDI of rescatter intermediate between SRFS and SRBS.

transverse velocity components may reach such energies, as may have occurred for L. Yin *et al.* [11], but we leave this for future work. For rescatter, on the other hand, with higher v_ϕ (and lower β), 100 keV is well within range. Rescatter EPWs, as well as their LDI decay EPWs, are potential producers of 100 keV electrons.

In this Letter, we present one- and two-dimensional (1D and 2D) simulations using the electromagnetic PIC code OSIRIS [12]. The first simulation is 1D with $T_e = 2.5$ keV, electron density $n_e/n_{\text{cr}} = 0.09$ ($k\lambda_D \approx 0.35$ for SRBS), and both fixed and mobile ions with $ZT_e/T_i = 3$ and $M_i/m_e = 1836$. The laser has a wavelength of $\lambda_0 = 0.351\,\mu$m and intensity $I_0 = 3 \times 10^{15}$ W/cm^2. The number of cells used was 16 384, with 512 particles per cell with quadratic particle shapes to simulate a plasma of length 180 μm corresponding to an $f/8$ speckle of length $8f^2\lambda_0 = 180\,\mu$m. The second simulation is exactly similar (with mobile ions), with the exception that it has a linear density gradient from $n_e/n_{\text{cr}} = 0.09$ to 0.10 over the domain length. Finally, the third simulation is 2D with $T_e = 3$ keV, $n_e/n_{\text{cr}} = 0.10$, $ZT_e/T_i = 2$, domain size $200 \times 15\,\mu\text{m}^2$, $16\,384 \times 512$ cells, 256 particles per cell, and the laser is focused from $I_0 = 3 \times 10^{15}$ W/cm^2 at the simulation edge to $I_0 = 5 \times 10^{15}$ W/cm^2 at focus with a focal spot size of 2.6 μm ($8\lambda_0$). All simulations have absorbing boundaries for the fields in all directions and have the plasma extending up to the boundary in all directions; exiting particles are reinjected with a random velocity from the initial background Maxwellian distribution. The laser propagates along $\hat{x}$, is polarized in $\hat{z}$ (perpendicular to the 2D plane), and has a constant amplitude after a rise time of $\omega_0 t_{\text{rise}} = 300$.

First, we consider the 1D run with immobile ions and homogenous density $n_e/n_{\text{cr}} = 0.09$. The temporal evolution of the SRS EPW wave numbers can be seen in Fig. 3, along with the corresponding temporal evolution of the electron distribution function. SRBS grows first, as it has the largest growth rate. SRFS follows, and soon afterwards the scattered light from both SRFS and SRBS has grown to sufficient amplitude that rescatter grows.

The hot electron tails in the distribution follow a different progression. The forward-traveling EPW phase momenta ($p_x/m_e c = \gamma v_\phi$) increase from SRBS (0.24) to SRBS of SRFS (0.40) to SRFS (2.6), with electrons at those speeds having kinetic energies as shown in Fig. 2. Electron trapping by SRBS is present at $\omega_0 t \approx 10\,000$; this process does not accelerate electrons above 70 keV. SRFS has grown to a mode amplitude greater than SRBS by $\omega_0 t = 20\,000$, but normalized to its wave breaking value it is smaller, so it does not trap particles and has no immediate effect on the hot electron tail. Electrons begin to be accelerated to energies above 70 keV by the rescatter that is growing at $\omega_0 t \approx 20\,000$, and by $\omega_0 t \approx 33\,000$ electrons have been accelerated to sufficient energies by the rescatter that SRFS can trap electrons, accelerating them beyond 250 keV all the way up to 1 MeV.

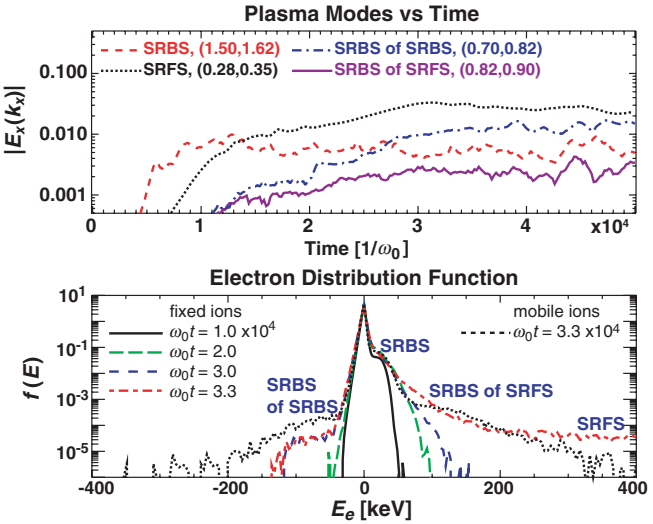

FIG. 3 (color). (top) Temporal evolution of the SRS EPW wave numbers for $k_x c/\omega_0$ within the labeled bounds; fixed ion simulation. (bottom) Electron energy spectrum; heating due to LDI not labeled.

Though not shown, the maximum EPW amplitude in the region of SRFS activity is $eE/m v_\phi \omega_p \approx e\Phi/m v_\phi^2 \approx 0.37$ at $\omega_0 t \approx 33\,000$. Using $v_\phi = 0.93c$, the energy an electron needs in order to be trapped is 140 keV ($v = 0.62c$). Since SRBS only generates electrons with energies less than approximately 70 keV, this illustrates why SRFS requires the intermediate step of rescatter. This is consistent with Fig. 3 where the hot tail sweeps to higher energies once rescatter heats electrons to 140 keV. With heating by both rescatter and SRFS, approximately 0.1% of the electrons get heated above 100 keV.

Figure 3 (bottom panel) also shows electron heating due to SRBS of SRBS in the negative direction with energies on the order of 100 keV. This tail requires longer to develop, as there is only one EPW in that direction and the rescatter must therefore be driven to sufficient amplitude.

The number of both forward and backward propagating EPWs is greater if we allow ions to be mobile. Figure 3 (bottom panel) shows a representative distribution from an equivalent simulation with mobile ions illustrating roughly similar electron heating, but the physics behind it is more complex due to LDI and the resulting counterpropagating EPWs that can be generated for each decaying EPW.

While we do not see Brillouin scattering for our parameters, we do see LDI. LDI can potentially saturate SRS, but each SRS process (SRBS, SRFS, and rescatter) has a different value of $k\lambda_D$ and is in a different kinetic regime. Both rescatter processes are SRBS processes and scale like SRBS, although the SRBS and SRFS scattered light waves have longer wavelengths and lower frequencies than the incident laser, resulting in comparatively lower SRBS intensity thresholds, higher growth rates, and rescattered EPWs less affected by kinetic effects and more affected by LDI. We have performed other simulations varying laser intensity, density, and temperature, and we have seen similar heating by rescatter provided the scattered light is intense enough. However, even for strong SRS, rescatter can not grow at densities above its quarter-critical density, which for scattered light of frequency $\omega \approx \omega_0 - \omega_p$ is $n/n_{\rm cr} \approx 0.11$. On the other hand, for lower densities such as $n/n_{\rm cr} < 0.09$, the growth rates of all SRS processes decrease, similarly making rescatter less likely; density gradients will also act to quench SRS instabilities.

We turn now to our second simulation setup, a scenario in which SRFS is quenched by the density gradient; density rises linearly from $n_e/n_{\rm cr} = 0.09$ to 0.10 over the domain length. Only one variety of rescatter is present (SRBS of SRBS). In this case, the impact of LDI is therefore simplified.

The spectrum of plasma modes can be seen in Fig. 4 (top). Figure 4 (bottom) shows that rescatter (here SRBS of SRBS) again accelerates electrons up to energies of 100–200 keV. The EPW from the LDI decay of rescatter also heats electrons, and as it travels in the opposite direction as the rescatter EPW, the combined instabilities generate energetic electrons in both directions. One reason that the electrons going forward reach higher energies than those going backward is because the LDI decay EPW has a slightly lower wave number compared to the rescatter EPW and therefore a slightly higher phase velocity. The hot tail due to LDI therefore extends to higher energies than the tail due to rescatter. Furthermore, even though the LDI EPW interacts with the electron distribution at higher

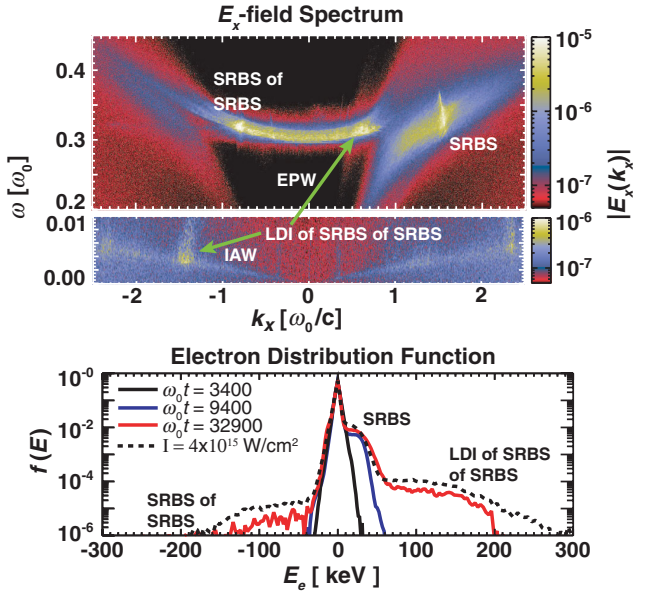

FIG. 4 (color). (top) Frequency vs wave number of E_x field. (bottom) Electron distribution vs electron kinetic energy for $I_0 = 3 \times 10^{15}$ (solid lines) and 4×10^{15} W/cm^2 (dashed line), where +/- represent forward/backward traveling electrons.

velocities, it heats more total electrons than the rescatter EPW since it also interacts with the previously formed hot tail from the original SRBS.

If we apply our earlier theoretical estimate of electron $v_{\max}$ to the rescatter and LDI EPWs, we can test it against the electron spectrum shown in Fig. 4. The EPWs have $v_\phi \approx 5.6 v_{\rm th}$ for rescatter of SRBS and $6.4 v_{\rm th}$ for LDI of rescatter. The electron kinetic energies corresponding to the theoretical limit (Fig. 2) of $v_{\max}$ are ≈ 200 keV for SRBS and 300 keV for LDI. These indeed bound the upper edges of the flat tails in the plotted distribution in Fig. 4, even for an exactly similar case with higher laser intensity. The low-velocity end of the hot tails corresponds approximately to $\mathcal{E}_\phi \approx mc^2(\gamma_\phi - 1)$ (≈ 44 and 61 keV).

Finally, we present results from a 2D simulation of a single speckle in a uniform plasma. Figure 5 (top left) shows the temporal evolution of wave numbers for the E_z (transverse) field along the central axis. The bursty mode at $kc/\omega_0 \approx 0.5$ corresponds to SRBS, whereas the steadily growing mode at $kc/\omega_0 \approx 0.6$ that peaks at $\omega_0 t \approx 17\,000$ corresponds to SRFS (the anti-Stokes mode is also present at $kc/\omega_0 \approx 1.3$). Rescatter of both light waves is present, with SRBS of SRBS at $kc/\omega_0 \approx 0.20$ and SRBS of SRFS at $kc/\omega_0 \approx 0.15$ starting at $\omega_0 t \approx 17\,000$. Corresponding rescatter plasma wave modes are seen in the E_x field (not shown) as well as broadband signals from modes that grow after $\omega_0 t \approx 17\,000$ due to LDI. SRBS EPWs

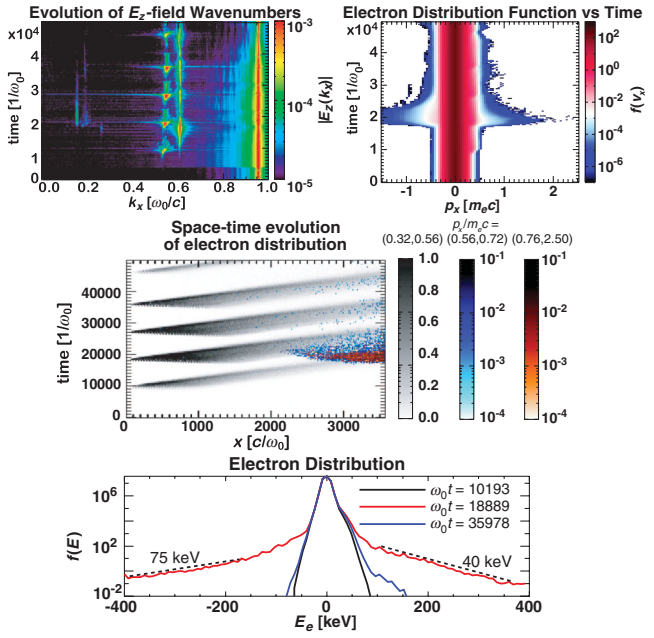

FIG. 5 (color). (top) Temporal evolution of transverse E-field wave numbers along the simulation center (top left) and longitudinal electron distribution spatially averaged over x and y (top right). (middle) Charge density of electrons at v_ϕ of SRBS (gray), SRBS of SRFS (blue), and SRFS (orange). (bottom) Energy distribution; includes transverse momentum with $\pm$ referring to the sign of p_x.

may be affected by 2D kinetic effects such as transverse localization, wave bowing, and filamentation [13–16], though the rescatter EPWs have $k\lambda_D \approx 0.2$ and are more affected by LDI. The study in detail of the interplay of these effects when such a wide variety of EPWs is present, each in a different kinetic regime, is left for future work.

The electron distribution shown in Fig. 5 (top right) flattens slightly at $\omega_0 t = 10\,000$ due to the first burst of SRBS, followed by much more energetic tails at $\omega_0 t = 18\,000$ due to rescatter and LDI of rescatter. Though not shown here, the electron phase space reveals that the positive momentum tail is caused by SRBS of SRFS and the negative momentum tail is caused by LDI of SRBS of SRFS. The importance of trapped electron bootstrapping between SRBS and rescatter can be seen in the middle plot of Fig. 5, where the charge density amplitude in electron phase space, summed over the transverse direction, is plotted as a function of space and time for three different ranges of electron momenta. The phase space bins $p_x/m_e c = (0.32, 0.56)$, (0.56, 0.72), and (0.76, 2.50) cover v_ϕ of the EPWs due to SRBS, SRBS of SRFS, and SRFS, respectively. With SRBS (SRFS) growing behind (in front of) the laser focus ($x\omega_0/c = 1790$), electrons heated by SRBS first have to cross the simulation length before interacting with the region where SRFS (and rescatter of SRFS) has grown. After they cross (as shown in gray), the rescatter can interact with these electrons and accelerate them further. Blue shows electrons heated by rescatter, which is seen to occur when electrons heated by SRBS enter the region of rescatter, whereas orange shows further acceleration by SRFS. LDI limits SRFS for $\omega_0 t > 20\,000$ and, thereby, also the rescatter of SRFS. At $\omega_0 t \approx 18\,000$, those hot electrons with kinetic energies above 100 keV have a forward-going kinetic energy flux of approximately 3% of the total incident laser Poynting flux, whereas subsequent fluxes at $\omega_0 t \approx 36\,000$ and $43\,000$ are both $\approx 0.2\%$.

The electron distribution in energy is shown in Fig. 5 (bottom), where one can see that electrons are not accelerated above 100 keV energies until rescatter has grown ($\omega_0 t > 17\,000$). Fitted lines for temperatures show that the range of electron energies, not the slope of the distribution, identifies which plasma wave (instability) is responsible for those hot electrons, a conclusion which could also be drawn from Figs. 3 and 4.

The range of energies shown in this Letter is consistent with reported hot electron measurements from NIF and shows that SRS rescatter should be considered as a source of 100 keV electrons. While the results here are limited to single speckles with intensities at the higher end of expected hot spot intensities (e.g., including cross-beam energy transfer and overlapping inner beams [17,18]), one might reasonably assume that scattered light will be amplified to levels seen here as it travels through multiple speckles. Multistage electron acceleration between EPWs has been shown in two-plasmon decay simulations [19]

and may generate 100 keV electrons in multispeckle SRS; we believe this topic is worth further study.

This work was supported by the DOE under Grants No. DE-FG52-09NA29552 and No. DE-NA0001833 and by the NSF under Grant No. NSF-Phy-0904039. Simulations were carried out on the UCLA Hoffman2 cluster and NERSC's Franklin and Hopper systems.

[1] E. L. Dewald *et al.*, Rev. Sci. Instrum. **81**, 10D938 (2010).
[2] P. Michel *et al.*, Phys. Rev. E **83**, 046409 (2011).
[3] D. E. Hinkel, S. W. Haan, A. B. Langdon, T. R. Dittrich, C. H. Still, and M. M. Marinak, Phys. Plasmas **11**, 1128 (2004).
[4] K. Estabrook, W. L. Kruer, and B. F. Lasinski, Phys. Rev. Lett. **45**, 1399 (1980); K. Estabrook and W. L. Kruer, Phys. Fluids **26**, 1892 (1983).
[5] W. B. Mori, M.S. thesis, University of California, Los Angeles, 1984.
[6] P. Bertrand, A. Ghizzo, S. J. Karttunen, T. J. H. Pattikangas, R. R. E. Salomaa, and M. Shoucri, Phys. Plasmas **2**, 3115 (1995).
[7] A. B. Langdon and D. E. Hinkel, Phys. Rev. Lett. **89**, 015003 (2002).
[8] T. P. Coffey, Phys. Fluids **14**, 1402 (1971).
[9] W. B. Mori and T. Katsouleas, Phys. Scr. **T30**, 127 (1990).
[10] More detail will be provided in a longer paper.
[11] L. Yin *et al.*, Phys. Plasmas **19**, 056304 (2012).
[12] R. G. Hemker. Ph.D. thesis, University of California, Los Angeles, 2000; R. A. Fonseca, L. O. Silva, F. S. Tsung, V. K. Decyk, W. Lu, C. Ren, and W. B. Mori, Lect. Notes Comput. Sci. **2331**, 342 (2002); R. A. Fonseca, S. F. Martins, L. O. Silva, J. W. Tonge, F. S. Tsung, and W. B. Mori, Plasma Phys. Controlled Fusion **50**, 124034 (2008).
[13] J. E. Fahlen, B. J. Winjum, T. Grismayer, and W. B. Mori, Phys. Rev. E **83**, 045401(R) (2011).
[14] J. Banks, R. L. Berger, S. Brunner, B. I. Cohen, and J. A. F. Hittinger, Phys. Plasmas **18**, 052102 (2011).
[15] L. Yin, B. J. Albright, K. J. Bowers, W. Daughton, and H. A. Rose, Phys. Plasmas **15**, 013109 (2008).
[16] H. A. Rose and L. Yin, Phys. Plasmas **15**, 042311 (2008).
[17] P. Michel *et al.*, Phys. Plasmas **17**, 056305 (2010).
[18] D. E. Hinkel *et al.*, Phys. Plasmas **18**, 056312 (2011).
[19] R. Yan, C. Ren, J. Li, A. V. Maximov, W. B. Mori, Z.-M. Sheng, and F. S. Tsung, Phys. Rev. Lett. **108**, 175002 (2012).